Cleaner Materials 10 (2023) 100209

Contents lists available at ScienceDirect

Cleaner Materials

journal homepage: www.journals.elsevier.com/cleaner-materials

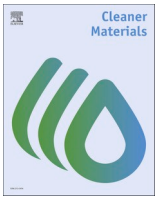

Ground granulated iron silicate slag as supplementary cementitious material: Effect of prolonged grinding and granulation temperature

Anton Andersson [a,*], Linus Brander [b], Andreas Lennartsson [a], Åke Roos [c], Fredrik Engström [a]

[a] Luleå University of Technology, Division of Minerals and Metallurgical Engineering, Luleå tekniska universitet, SE-971 87 Luleå, Sweden
[b] Research Institute of Sweden, Division of Built Environment – Infrastructure and Concrete, Box 857, SE-501 15 Borås, Sweden
[c] Boliden Smelters, Boliden AB, Klarabergsviadukten 90, SE-101 20, Stockholm, Sweden

ARTICLE INFO

Keywords:
Iron silicate slag
Copper slag
Supplementary cementitious material
Recycling
Circularity

ABSTRACT

The metallurgical and cement industries contribute significantly to anthropogenic carbon dioxide emissions. Utilizing oxidic by-products from the metallurgical industry as supplementary cementitious materials (SCMs) can improve resource efficiency and reduce emissions from cement production. Iron silicate copper slags have been studied as SCMs, but mainly in systems where Portland cement is used as an activator. There is limited research on the inherent reactivity of the slag under changing processing conditions. The present study offers insight into the effect of granulation temperature and grinding on the inherent reactivity of an industrially produced iron silicate copper slag. The results showed that granulation temperature had an insignificant effect on reactivity, while grinding generated substantial improvements. The latter effect was concluded to stem from the increased specific surface area, increased number of sites for nucleation and growth of hydrates, and changes in the inherent reactivity owing to structural changes induced by the grinding.

1. Introduction

The cement and metallurgical industries account for a substantial part of the anthropogenic carbon footprint. Previous publications state that the contribution of the cement industry amounts to 5–8 % of global carbon dioxide emissions (Benhelal et al., 2021; Olivier et al., 2012). In comparison, copper production has a lower share, approximately 0.3 %, as calculated by Watari et al. (Watari et al., 2022) using the data presented by Hertwich (Hertwich, 2021). However, each ton of produced copper generates, on average, 2.2 to 3.0 tons of slag (Gabasiane et al., 2021; Shi et al., 2008), which must be utilized to ensure sustainable copper production from a resource-efficiency standpoint. Fig. 1 illustrates that the generation of copper slag spans all inhabited continents, which suggests that measures taken to valorize the slag have a global impact.

Several external applications for copper slag have been reported, e.g., various construction applications excluding cement and concrete (Gabasiane et al., 2021; Shi et al., 2008; Kero Andertun et al., 2022; Murari et al., 2015), blasting abrasive media (Shi et al., 2008; Kero Andertun et al., 2022; Murari et al., 2015; Al-Jabri et al., 2006), auxiliary sand in concrete (Gabasiane et al., 2021; Shi et al., 2008), and for its pozzolanic properties, i.e., as s upplementary cementitious material (SCM) (Gabasiane et al., 2021; Shi et al., 2008). Although options for utilization in external applications have been reported, one observation from the review by Gabasiane et al. (Gabasiane et al., 2021) was that many smelters landfill the slag due to environmental concerns. Thus, in accordance with the results presented by Kero Andertun (Kero Andertun et al., 2022; Kero Andertun et al., 2022), improved slag cleaning operations should be emphasized to reach an environmentally safe product, which will enable utilization in external applications.

Of the abovementioned uses of the slag, an attractive alternative is utilization as an SCM, which would improve the resource efficiency while simultaneously lowering the carbon dioxide emissions per ton of cementitious material. The former effect is obvious, i.e., lower requirements for the quarrying of virgin material, while the latter relates to the fact that the SCM does not require additional calcination (release of chemically bound carbon dioxide) and clinkering (Lothenbach et al., 2011). Tixier et al. (Tixier et al., 1997) published a study on the partial replacement of Portland cement with iron silicate copper slag in 1997. Although, at this time, the study was motivated by eliminating disposal costs related to the slag (Tixier et al., 1997) rather than emissions from cement production. Nonetheless, the results showed that the

* Corresponding author.
E-mail addresses: anton.andersson@ltu.se (A. Andersson), linus.brander@ri.se (L. Brander), andreas.lennartsson@ltu.se (A. Lennartsson), ake.roos@boliden.com (Roos), fredrik.i.engstrom@ltu.se (F. Engström).

https://doi.org/10.1016/j.clema.2023.100209
Received 26 June 2023; Received in revised form 6 September 2023; Accepted 12 October 2023
Available online 14 October 2023

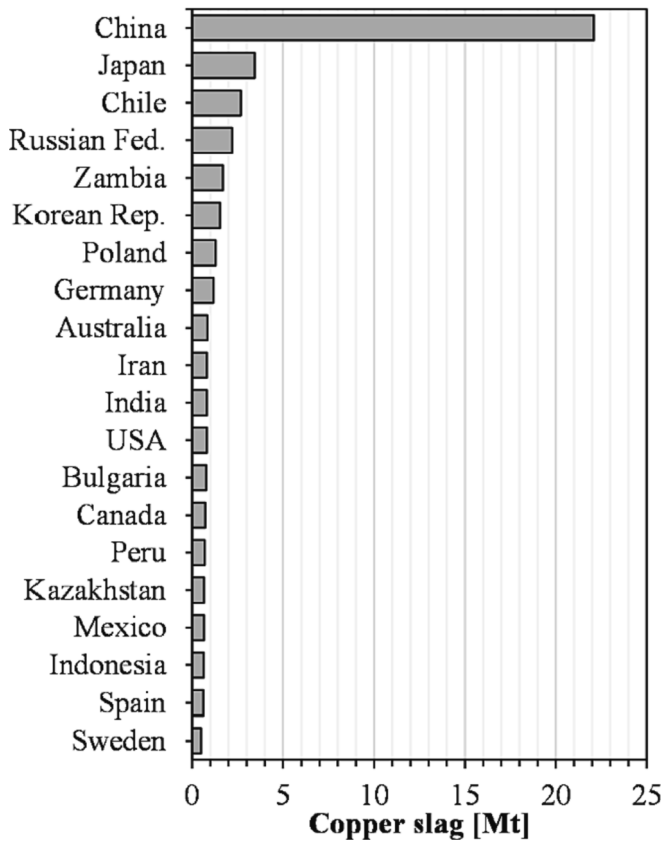

Fig. 1. Estimated copper slag generation for the top 20 nations ranked by copper smelter production. Combined data from (Gabasiane et al., 2021; Shi et al., 2008; International Copper Study Group, The World Copper Factbook, 2022).

incorporation of the slag improved the compressive strength of mortars after curing beyond seven days (Tixier et al., 1997).

Since 1997, several studies have been published explicitly addressing iron silicate copper slags for SCM applications (Al-Jabri et al., 2006; Moura et al., 2007; de Rojas et al., 2008; Singh et al., 2016; Edwin et al., 2016; Sheng et al., 2016; Sivakumar et al., 2019; He et al., 2021; Wang et al., 2020; Feng et al., 2019; Feng et al., 2019). Furthermore, additional studies have incorporated the slag to compare different SCMs (Sivakumar et al., 2021). The slag compositions included in these studies are presented in Table 1. Furthermore, the primary methodologies employed include mortar testing (Al-Jabri et al., 2006; Moura et al., 2007; de Rojas et al., 2008; Singh et al., 2016; Edwin et al., 2016; Sivakumar et al., 2019; Wang et al., 2020; Sivakumar et al., 2021), cement composite testing (He et al., 2021; Feng et al., 2019; Feng et al., 2019), isothermal calorimetry on Portland cement blends (de Rojas et al., 2008; Edwin et al., 2016; Feng et al., 2019; Feng et al., 2019), isothermal calorimetry using the R^3 test (Sivakumar et al., 2021), as well as the Chapelle and Frattini tests (Edwin et al., 2016).

In comparison to the work published in 1997 (Tixier et al., 1997), the reported data is ambiguous in terms of the strength of mortars with iron silicate copper slag partially replacing Portland cement. Moura et al. (Moura et al., 2007) reported that both the compressive strength and splitting tensile strength improved by replacing 20 % of the Portland cement. The mechanism of improvement was argued to be caused by the enhanced formation of the calcium silicate hydrate (C-S-H) gel and the filler effect (Moura et al., 2007). Singh et al. (Singh et al., 2016) made similar observations; the compressive and flexural strength improved with added slag, provided the samples were cured for at least 90 days. Other studies suggest that the strength decreases when compared to mortars without partial replacement of the Portland cement (Al-Jabri et al., 2006; de Rojas et al., 2008; Edwin et al., 2016; Sivakumar et al., 2019). However, owing to the pozzolanic activity of the slag—that has been shown with dedicated testing (de Rojas et al., 2008; Edwin et al., 2016; Sheng et al., 2016; Sivakumar et al., 2019; Sivakumar et al., 2021)—the decrease in strength is smaller than the percentage of cement replaced (de Rojas et al., 2008; Sivakumar et al., 2019). The same conclusion can be made based on the data presented by Edwin et al. (Edwin et al., 2016) for high replacement rates and long curing times, as well as for the cement composites studied by both He et al. (He et al., 2021) and Feng et al. (Feng et al., 2019).

The somewhat inconsistent results highlight that several aspects affect the performance of SCMs, e.g., degree of crystallinity, granulometric properties, and chemical composition (Ramanathan et al., 2021; Ramanathan et al., 2022; Zhang et al., 2011; Mirzahosseini and Riding, 2015; Schöler et al., 2017; Snellings, 2013; Bignozzi et al., 2015), which, naturally, have not been constant between the different studies. In addition, studies on mortars and composites have reported different replacement ratios. Tested replacement ratios of cement with copper slag span from 5 to 50 % (Tixier et al., 1997; Moura et al., 2007; de Rojas et al., 2008; Singh et al., 2016; Edwin et al., 2016; Sivakumar et al., 2019; Feng et al., 2019; Sivakumar et al., 2021), and the local maximum in terms of performance has been reported within the range of 10–20 % replacement (Moura et al., 2007; Singh et al., 2016; Edwin et al., 2016; Sivakumar et al., 2021). Nonetheless, most studies point out that the slag can be successfully applied as an SCM when accounting for the replacement ratio of Portland cement. This conclusion reflects the results of Wang et al. (Wang et al., 2020), finding that ten different copper slags with different chemical compositions produced by both air cooling and water granulation, and consequently with different degrees of crystallinity, all contributed to the strength when accounting for the replacement ratio.

If a smelter aims at a particular slag composition appropriate for its

Table 1
Summary of slag compositions evaluated for SCM purposes in the literature. The reported concentrations [wt%] were rounded to one decimal point. The FeO/SiO_2 ratio was, however, calculated based on the reported values from the authors.

Ref.	FeO/SiO_2	FeO*	SiO_2	CaO	Al_2O_3	MgO	ZnO*	Cu*
(He et al., 2021)	1.12	37.9	33.9	12.7	4.7	0.8	/	/
(Feng et al., 2019)	1.14	37.9	33.3	12.3	4.6	1.1	1.3	1.4
(Feng et al., 2019)	1.14	36.9	32.3	19.5	3.9	0.9	1.2	1.2
(Sivakumar et al., 2019; Sivakumar et al., 2021)	1.14	36.8	32.3	3.9	11.0	/	/	/
(Feng et al., 2019; Feng et al., 2019)	1.27	42.3	33.4	4.0	3.5	1.4	1.1	/
(Tixier et al., 1997)	1.35	47.5	35.2	3.3	5.0	0.6	/	0.5
(Al-Jabri et al., 2006)	1.46	48.1	33.1	6.1	2.8	1.6	/	0.4
(Sheng et al., 2016)	1.49	46.9	31.5	3.2	8.5	4.4	0.3	1.3
(Edwin et al., 2016)	1.58	40.9	25.9	7.1	5.9	0.8	8.8	0.3
(de Rojas et al., 2008)	1.80	54.0	30.1	0.6	4.0	0.8	/	/
(Singh et al., 2016)	1.98	55.5	28.0	2.5	4.0	1.2	/	0.7
(Moura et al., 2007)	2.15	56.0	26.0	2.0	3.3	2.7	0.9	1.1

*Analyses given for different oxidation states (0, +I, +II, or + III) were recalculated to FeO, ZnO, and Cu to enable the comparison.

operation from a metallurgical standpoint, two main parameters can be addressed to influence the suitability of the slag as an SCM. Firstly, the cooling procedure, which translates to the degree of crystallinity of the slag (Wang et al., 2020) and possibly the polymerization (Stebbins, 1988). Secondly, the subsequent milling of the slag, which determines the specific surface area and may result in the amorphization of crystalline phases by mechanical activation (Feng et al., 2019). Although extended milling has been performed on granulated iron silicate copper slag (Feng et al., 2019), the effect on the inherent reactivity of the slag after such tests has not been reported. Instead, Portland cement was used as an activator for the slag (Feng et al., 2019), which, as discussed by Sivakumar et al. (Sivakumar et al., 2021), renders the conclusions on inherent reactivity merely speculative.

In the present study, a water-granulated iron silicate slag was investigated for its inherent reactivity as an SCM. More specifically, the processing conditions for a fixed chemical composition were addressed by studying prolonged grinding and the effect of cooling conditions on the reactivity. As attaining an amorphous slag is desirable for the SCM application, the parameter addressed in the cooling process was granulation temperature, which has not been studied for iron silicate copper slags before.

2. Materials and methods

A spot sample of water-granulated copper slag from Boliden Rönnskär, Sweden, was used in the present study. The slag was a fumed and settled iron silicate copper slag sampled after the dewatering process (as illustrated in the flow sheet of Isaksson et al. (Isaksson et al., 2021). After sampling, the material was dried and split into representative subsamples using a Jones riffler. Each experiment or analysis presented in the text below was performed on such a subsample.

2.1. Characterization and calorimetry-based testing

The chemical composition of the slag was determined by X-ray fluorescence (XRF) spectrometry on a pressed powder sample. For the analysis, a SPECTRO XEPOS energy dispersive XRF spectrometer (SPECTRO, Kleve, Germany) equipped with a binary palladium-cobalt anode was used. The instrument was calibrated with in-house standard samples from Boliden Rönnskär.

Powder X-ray diffraction (XRD) was used to determine the mineralogical composition of the slag. The sample was scanned between 10 and 90 °2θ with copper K_α generated at 45 kV and 40 mA using a Malvern Panalytical Empyrean X-ray diffractometer (Malvern Panalytical, Malvern, United Kingdom). Furthermore, the fraction of amorphous material in the sample was determined using Rietveld XRD with an internal standard. Based on possible present phases, calcite (99.5 % $CaCO_3$) was determined to be a suitable internal standard to avoid overlapping peaks. In accordance with published literature (Ramanathan et al., 2021; Moon et al., 2016; Astoveza et al., 2022), the chosen internal standard was mixed to obtain 10 wt% in the sample. Mixing was made using a ring mill, and the subsequent scan was performed in accordance with the above. The refinement was performed using HighScore + and the COD database (Grazulis et al., 2009).

Before the isothermal calorimetry experiment, the sample was milled in a FRITSCH Pulverisette 7 planetary ball mill (FRITSCH GmbH, Idar-Oberstein, Germany) using tungsten carbide (WC) grinding bowls. Two separate cycles were employed to reach a fine particle size distribution without excessive time spent under grinding: i) a 3 min cycle of coarse grinding at 600 revolutions per minute (RPM) using 7 WC balls of 15 mm in diameter, and ii) a fine grinding cycle of 1 min at 600 RPM using 180 WC balls of 5 mm in diameter. The coarse grinding was based on roughly 12 mL of a representative sample of slag granules, and the fine grinding was, subsequently, performed on the material from the first step.

The ground iron silicate slag was subjected to the isothermal calorimetry-based rapid screening test for SCMs outlined by Snellings and Scrivener (Snellings and Scrivener, 2016), further developed and referred to as the rapid, relevant, and reliable (R^3) test by Avet et al. (Avet et al., 2016). The choice of this method was based on the study presented by Li et al. (Li et al., 2018), which demonstrated that the R^3 test results correlated strongly to the strength of mortars, independent of the type of SCM and with great repeatability between laboratories. Furthermore, this calorimetry-based testing method tests the inherent reactivity of the SCM without the influence of cement hydration (Sivakumar et al., 2021; Hallet et al., 2020).

A 3:1 mass-based ratio between portlandite (98 % $Ca(OH)_2$) and the ground slag was mixed together with potassium sulfate (99.99 % K_2SO_4) on a dry basis. The amount of potassium sulfate was based on the analyzed alumina content of the slag to achieve a 1:1 SO_3:Al_2O_3 molar ratio. A paste with a 1:1 mass-based ratio of 0.5 M potassium hydroxide solution and the solid blend was mixed for 2 min at 1600 RPM using an overhead stirrer. About 15 g of the paste was transferred to a calorimeter glass ampoule and subsequently placed in a TAM Air isothermal calorimeter (TA Instruments, New Castle, Delaware, USA). The sealed ampoule was placed in the calorimeter within 5 min after adding the potassium hydroxide solution to the solid blend. The heat flow was recorded for 28 days at a temperature of 40 °C. All weights were recorded on the third decimal point.

Due to the importance of the granulometric properties of SCMs (Ramanathan et al., 2021; Ramanathan et al., 2022; Zhang et al., 2011; Mirzahosseini and Riding, 2015), the ground sample was characterized for its particle size distribution using laser diffraction by employing a Malvern Mastersizer 3000 (Malvern Panalytical, Malvern, United Kingdom). The measurements were performed in an ultrasound-dispersed water suspension, and the results were evaluated using the Fraunhofer approximation. Furthermore, the Brunauer, Emmett, and Teller (BET) specific surface area of the ground sample was determined with a Micromeritics Gemini 2390a operating on nitrogen after degassing at 300 °C for 60 min using a Micromeritics FlowPrep 060 (Micromeritics Instruments Corporation, Norcross, Georgia, USA).

2.2. Effect of prolonged grinding

To study the influence of grinding on the performance of the iron silicate slag as an SCM, a series of grinding experiments were conducted. Each sample was subjected to a coarse grinding step of 3 min using the 15 mm diameter WC ball media. After the initial grinding, a second grinding process using the 5 mm diameter WC ball media was performed. Both operations were carried out at 600 RPM, and the second step was carried out for successively longer durations in accordance with the information presented in Table 2. The sample labeled Grinding 1 is the same sample described in **Section 3.1**.

Each sample presented in Table 2 was subjected to the previously described methods, i.e., the R^3 isothermal calorimetric test, laser diffraction analysis, BET specific surface area measurement, and XRD without internal standard.

In addition, selected samples were subjected to measurements using differential scanning calorimetry (DSC) in a Netzsch STA409 with Pt/Rh

Table 2
First (middle column) and second (right column) grinding stages used in the study.

Label	15 mm WC media [min]	5 mm WC media [min]
Grinding 1	3	1
Grinding 2	3	3
Grinding 3	3	6
Grinding 4	3	9
Grinding 5	3	12
Grinding 6	3	24
Grinding 7	3	48

pans. The heat capacity at constant pressure (C_p) was determined using a C_p triplicate, i.e., a correction file, a reference sample of sapphire, and a scan of the actual sample. The samples were subjected to an upscan from 373 K to 1200 K, a subsequent downscan to 373 K, a settling time for the temperature of 20 min, and a second upscan to 1200 K, each performed at a heating or cooling rate of 10 K/min.

2.3. Effect of granulation temperature

Increasing temperatures of silicate melts have been shown to provide similar changes in structure as the addition of network modifiers (Stebbins, 1988). Furthermore, network modifiers may alter the reactivity of an amorphous phase in pore solution conditions (Schöler et al., 2017; Snellings, 2013). Therefore, as the temperature is a viable process parameter at smelters, the effect of granulation temperature on reactivity was studied.

Subsamples of the industrial slag were remelted under an inert gas atmosphere in a graphite resistance-heated furnace (Ruhstrat, Göttingen, Germany), Fig. 2. The atmosphere was attained by injecting nitrogen (99.996 % N_2) and argon (99.999 % Ar) at flow rates of 12 L/min and 3 L/min ambient temperature and pressure, respectively. The choice of the crucible was based on the origin of the slag. In the industrial process, the slag undergoes a smelting reduction process driven close to the precipitation of metallic iron. Therefore, the partial pressure of oxygen set by contact with an iron crucible (>99.82 % Fe) closely resembles that of the industrial process, as the crucible acts as an oxygen buffer (Mysen and Richet, 2018).

Three samples were generated, each distinguished by their designated temperature in the furnace, i.e., 1473, 1573, and 1673 K. In the experiments, a fixed heating rate of 10 K/min was used, and, when reaching their final temperature, the slags were homogenized for 120 min. After this period, the iron crucible was removed from the furnace, and the slag was tapped and quenched in water jets operating with cold tap water at a rate of 1.1 L/s. The time between the removal of the sample from the furnace and the start of granulation was kept within 15 s. The sole condition changed for these experiments was the homogenization temperature in the furnace, which aimed at representing different operational temperatures at a smelter. The chosen nomenclature for the altered parameter in the present study was granulation temperature, which refers to the remelting temperature prior to the water granulation.

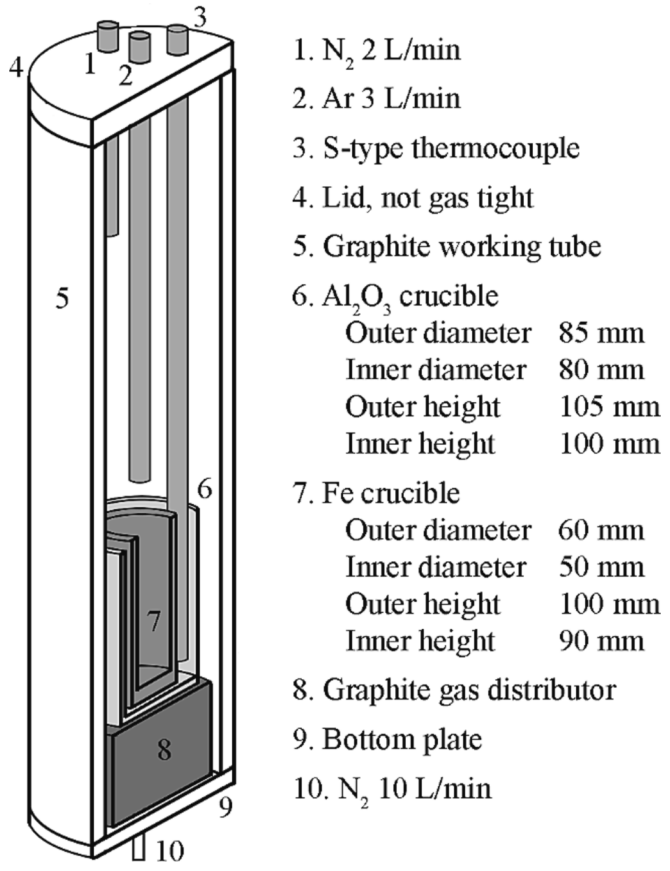

Fig 2. Overview of the experimental setup.

Each granulated sample was subjected to the grinding procedure equivalent to the sample labeled Grinding 1, Table 2. The ground slags were analyzed using the R^3 isothermal calorimetric test (for 7 days), laser diffraction, BET specific surface area measurements, DSC, and Rietveld XRD with the internal standard in accordance with previous descriptions.

3. Results and discussion

3.1. Chemical composition

The concentrations of the major constituents in the slag are presented in Table 3. As previously stated, prior to water granulation, the slag undergoes a reduction process to remove zinc. As the reduction progresses to partial pressures of oxygen close to the reduction of ferrous iron to metallic iron, the analysis in Table 3 is presented as ferrous iron rather than ferric. The chemical composition of the sample is within normal variations at the smelter, and, as such, the sample offers a baseline for evaluating its performance as an SCM.

Compared to previously studied iron silicate copper slags, the current slag is in the lower spectrum of the FeO/SiO_2 ratio; compare 1.14, calculated from Table 3, to the values presented in Table 1. In essence, this means that more silica could be available to participate in forming the C-S-H gel per mass unit dissolved SCM. Lothenbach et al. (Lothenbach et al., 2011) outlined that silica in SCMs consumes portlandite, generating progressively lower C/S ratios in the C-S-H gel with increasing amounts of silica reacting.

In terms of iron, several studies have found this element intermixed in the C-S-H gel (de Rojas et al., 2008; Sheng et al., 2016; Astoveza et al., 2022), but its contribution to gel formation is not fully understood (Astoveza et al., 2022; Hallet et al., 2020). A nuanced discussion on the topic of iron was provided by Peys et al. (Peys et al., 2022). In addition to differences in the gel formation, changing the FeO/SiO_2 quotient may affect the dissolution kinetics of the slag in the pore solution conditions since the degree of polymerization influences the dissolution behavior of amorphous phases (Schöler et al., 2017; Snellings, 2013). Therefore, a more depolymerized glass, i.e., a higher FeO/SiO_2 ratio, may provide more silica for the C-S-H gel due to improved dissolution kinetics.

The composition of the slag also classifies on the lower end of calcium oxide concentrations, especially for the slags with low FeO/SiO_2 ratios, Tables 1 and 3. Increasing concentrations of calcium oxide in

Table 3
Normalized chemical composition of the sample (note roundoff error to 100.1%).

Compound	Concentration [wt.%]
FeO	46.2
SiO_2	40.7
Al_2O_3	5.2
CaO	2.9
MgO	1.3
ZnO	1.2
Cu	0.8
Na_2O	0.7
K_2O	0.6
S	0.3
Cr_2O_3	0.2

synthetic glasses have been shown to improve dissolution in dilute suspensions in potassium hydroxide solution with pH values representing pore solution conditions (Schöler et al., 2017). These observations are consistent with the results presented by Feng et al. (Feng et al., 2019), showing that calcium oxide is positive in terms of strength development in cement composites with iron silicate slag.

Another major constituent is alumina, whose role in blends of Portland cement and ground granulated blast furnace slag (GGBS) was briefly outlined by Lothenbach et al. (Lothenbach et al., 2011). However, no studies could be found in the literature addressing the effect of alumina concentration of iron silicate slags on the reactivity in SCM applications, which is a relevant topic due to increasing loads of aluminum in copper smelters (Tian et al., 2022). Nonetheless, the alumina content of the slag in the present study, Table 3, is above the average reported value, Table 1, which may prove beneficial as Schöler et al. (Schöler et al., 2017) reported improved dissolution kinetics of synthetic glasses with increasing alumina contents. Furthermore, a more detailed assessment can be found in the work by Zhang et al. (Zhang et al., 2022), showing that the onset of aluminate reaction in a C_3S-gypsum-slag system is independent of slag alumina content. However, the subsequent rate of reaction depends on the availability of SO_4^{2-} and Al^{3+}, attributed to the gypsum and slag, respectively. Therefore, higher alumina contents in iron silicate slags might pose beneficial as a higher concentration can increase the availability of Al^{3+}.

In conclusion, the chemical composition of the slag is within the boundaries of previously studied compositions when considering each component individually. However, the composition is unique as a whole. Furthermore, the comparison highlights the need for controlled studies on the effect of chemical composition on the inherent reactivity of iron silicate copper slags. Placing the composition in its context in comparison to previously studied slags reveals that controlled studies for this specific system are yet to be performed.

3.2. Mineralogical composition

The scientific literature is clear on the differences in participation in s upplementary cementitious reactions for amorphous phases as opposed to crystalline phases, which was summarized by Kucharczyk et al. (Kucharczyk et al., 2018). More specifically, only a few crystalline phases, such as zeolites (Snellings, 2013) and certain minerals in calcareous fly ashes (Kucharczyk et al., 2018), show pozzolanic behavior. Otherwise, crystalline material has little to no contribution to the reactivity of SCMs (Snellings, 2013; Kucharczyk et al., 2018; Glosser et al., 2021).

The XRD analyses of the present study were performed to assess if the elements of the slag were available for participation in cementitious reactions. Based on the diffractogram without internal standard, Fig. 3 **a)**, tendencies towards crystallizing silica polymorphs are evident. Thermodynamically, this is expected due to the low FeO/SiO_2 ratio. Considering that, e.g., quartz can be mechanochemically activated by grinding (Yao et al., 2020), the crystallization may not be detrimental, although a fully amorphous material is preferred.

By including the internal standard and prolonging the scan time to acquire data for Rietveld refinement, the diffractogram presented in Fig. 3 **b)** was acquired. The approach plainly illustrates that the sample is dominated by amorphous material and that the presence of tridymite was below the quantification limits of the present setup.

3.3. Calorimetry-based testing

The grinding prior to the isothermal calorimetry-based testing generated a material with a d_{50} of 14 μm and a specific surface area of 0.62 m^2/g. Fig. 4 illustrates the first seven days of the R^3 experiment, and the results of the first 14 h indicate a strong heat release, possibly due to a high initial dissolution rate reflecting the almost completely

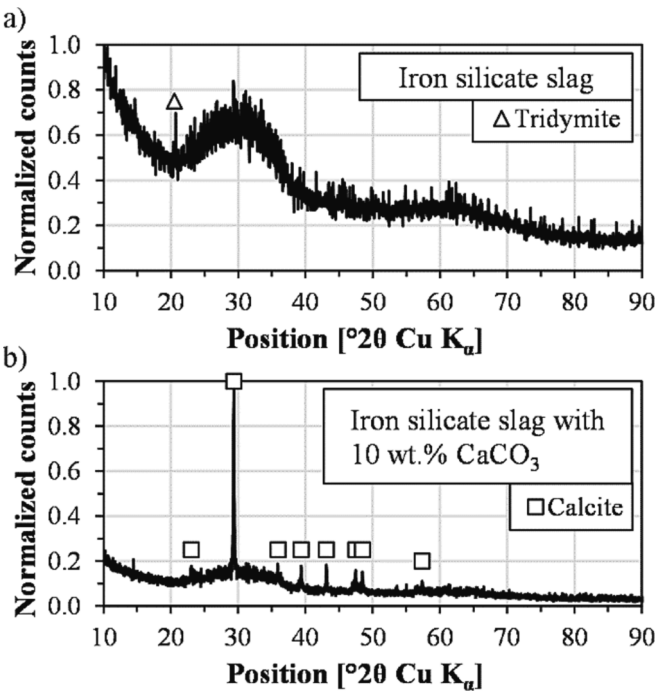

Fig. 3. Diffractogram of the slag **a)** without internal standard and **b)** with internal standard.

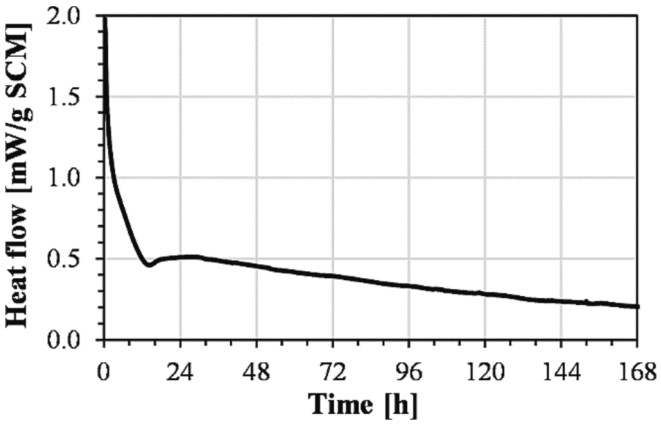

Fig. 4. Measured heat flow during the first 7 days of the R^3 protocol.

amorphous nature of the slag. During the dissolution, the released ions contributed to additional heat generation from the phase assemblage, which, according to previously reported data (Sivakumar et al., 2021; Hallet et al., 2020), could constitute phases such as C-S-H and calcium aluminum silicate hydrate (C-A-S-H) gel as well as alumina ferric oxide tri-substituted (AFt) and monosubstituted (AFm). Assuming that the slag dissolves congruently, which is likely based on data from other amorphous materials (Snellings, 2013), the slight increase in heat flow observed after 14 h is more realistically related to phase assemblage rather than dissolution of a specific component.

The gradual decline in the heat flow after 28 h, Fig. 4, suggests that the SCM is progressively consumed. However, the continuous contribution to the cumulative heat after 7 days, Fig. 5, indicates that the initial reaction rate is less than for, e.g., GGBS and calcined clay, both of which showed plateaus within 7 days of hydration (Snellings and Scrivener, 2016). Thus, the iron silicate slag of the present study takes a longer time to consume entirely and may contribute to the strength development in its application after prolonged hydration ages. This

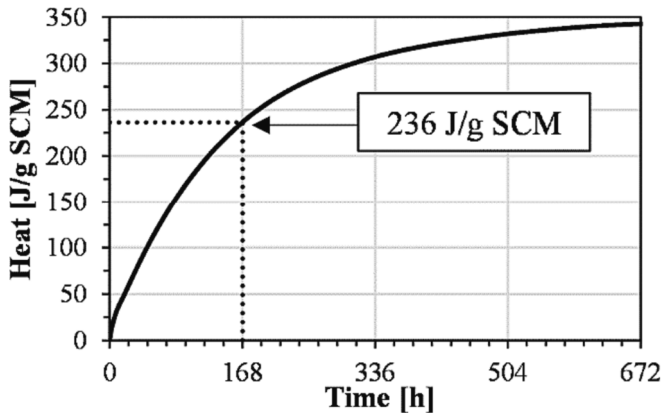

Fig. 5. Cumulative heat during the 28 days measurements in the R^3 protocol.

observation is consistent with the literature, where the effect of partially replacing Portland cement with iron silicate copper slag was reported to be more positive after a longer curing time (Tixier et al., 1997; de Rojas et al., 2008; Singh et al., 2016; Sivakumar et al., 2019; He et al., 2021; Wang et al., 2020; Feng et al., 2019; Feng et al., 2019).

The cumulative heat development measured in the R^3 test after 7 days, presented in Fig. 5, indicates that the performance of the iron silicate slag compares well to certain established categories of SCM. More specifically, fly ashes report values in the range of 173–180 (Snellings and Scrivener, 2016; Gholizadeh Vayghan et al., 2021), and Snellings et al. (Snellings and Scrivener, 2016) reported that a natural pozzolan generated 248 J/g SCM. Data on iron silicate copper slags are scarce, but the value presented in Fig. 5 is in the range of the non-ferrous slags reported by Hallet et al. (Hallet et al., 2020), which generated 201–240 J/g SCM. The literature also reports values of more reactive SCMs, such as GGBS and calcined clay, which have values from 492 to 518 and 574–935 J/g SCM, respectively (Snellings and Scrivener, 2016; Gholizadeh Vayghan et al., 2021). In this comparison, the particle size distribution and specific surface area were disregarded, the importance of which can not be understated due to the correlations between reactivity and granulometric properties reported in the literature (Ramanathan et al., 2021; Ramanathan et al., 2022; Zhang et al., 2011; Mirzahosseini and Riding, 2015; Yao et al., 2020; Shi et al., 2005).

Considering that certain elements have documented benefits in SCMs (Lothenbach et al., 2011; Feng et al., 2019; Schöler et al., 2017), changing the chemical composition of the slag could be a viable approach to improve its reactivity. However, there are additional processing parameters that can be considered to address the reactivity of the slag as an SCM, e.g., prolonged grinding.

3.4. *Effect of prolonged grinding*

High-energy grinding of crystalline-containing materials using, e.g., planetary ball mills, have been documented to cause amorphization and improve reactivity in, e.g., mine tailings, quartz as well as iron silicate slag with crystallized fayalite and magnetite (Feng et al., 2019; Ramanathan et al., 2021; Yao et al., 2020). This form of mechanochemical activation improves the reactivity in SCM applications based on the increased surface area induced by the comminution as well as local amorphization, disturbance in structural stability, and introduction of defects (Ramanathan et al., 2021). In the present study, the original slag was, in essence, entirely amorphous, and the prolonged grinding did not generate any shift in the amorphous hump nor any crystallization, Fig. 6. However, the tridymite was not observed after the first grinding step; compare Fig. 3 **a)** after ring mill against Fig. 6 after ball milling.

On the other hand, significant changes in the granulometric characteristics were generated, Fig. 7. The effect of grinding on the d_{50} can be summarized as an initial decline followed by a continuous increase.

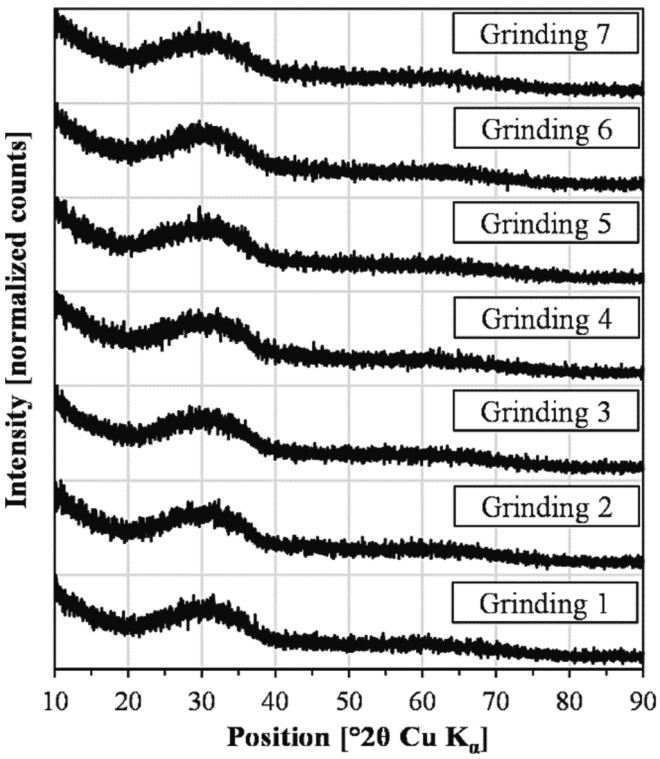

Fig. 6. Diffractograms recorded for milled slag samples.

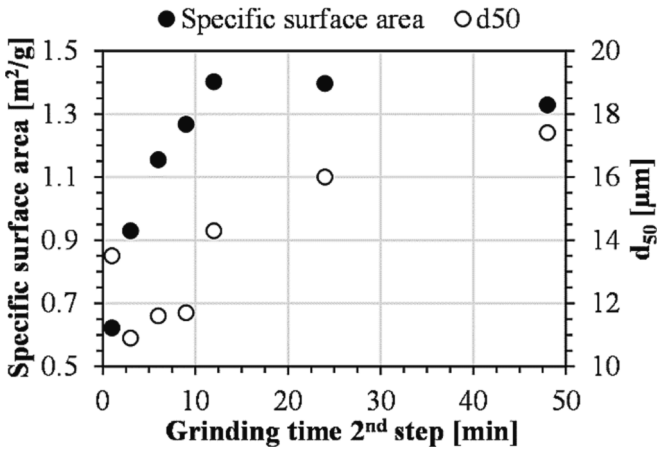

Fig. 7. Effect of prolonged grinding on the specific surface area and d_{50}.

Therefore, as the specific surface area increased up to 12 min of grinding, the particle breakage occurred mainly for particles above the d_{50} size range. For excessive grinding, minor agglomeration was observed, see Fig. 7, which is in accordance with the results of Romero Sarcos et al. (Romero Sarcos et al., 2021) in their study of GGBS.

Fig. 8 **a)** illustrates the correlation between evolved heat in the R^3 test and the specific surface area generated by the grinding. In the assessment, the 28 day heat was chosen as the results in Fig. 5 showed considerable contributions to the cumulative heat after 7 days of hydration. The results presented in Fig. 8 **a)** are in line with a well-known concept for SCMs, i.e., the reactivity increases with increased surface area (Skibsted and Snellings, 2019).

The juxtaposition of the data in Fig. 8 **a)** and **b)**, in particular related to the specific surface area, provides an interesting observation. Although the absolute reactivity, i.e., normalized against mass, improves with increased surface area, the evolved heat normalized against

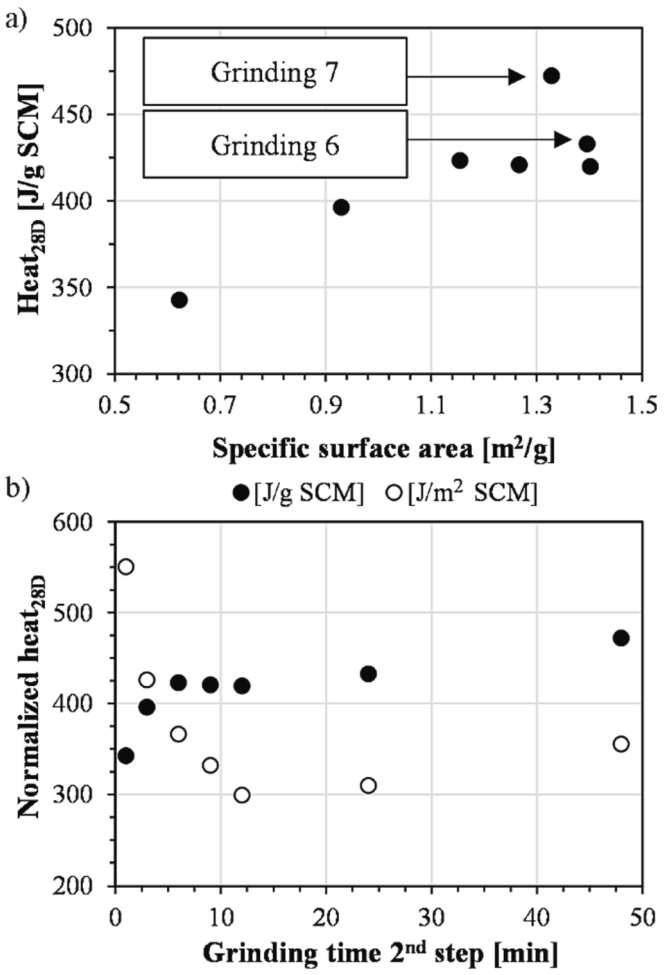

Fig. 8. A) Evolved heat after 28 days vs. specific surface area. **b)** Evolved heat after 28 days vs. grinding time in the second grinding step.

the generated surface area generally decreases with prolonged grinding. This means that the relative improvement in reactivity is less compared to the relative increase in generated surface area.

The previous paragraph disregards the kinks in the datasets presented in Fig. 8 in relation to increasing the grinding beyond 12 min. From an arithmetic standpoint, the effect is simple, i.e., there is a slight decrease in specific surface area due to agglomeration effects while, simultaneously, the reactivity improves. In accordance with the discussion by Ramanathan et al. (Ramanathan et al., 2021), separating the actual effect of grinding and granulometric properties requires sieving and testing an equivalent fraction after different grinding procedures. Although this method was not employed in the present study, the results indicate that extended grinding generates effects that improve the reactivity of the slag. Assuming, again, that the glass dissolves congruently, according to the observations by Snellings (Snellings, 2013), the higher observed heat evolution in J/g translates directly to improved dissolution of the slag particles.

Fig. 9 compares the early heat generation of four selected samples: i) the lower extreme, ii) the first sample in the plateau of Fig. 8 **b)**, iii) the first sample to break the plateau, and iv) the upper extreme. As indicated by Fig. 9, the onset of events differs significantly in time owing to changes induced by the grinding. The reduction in size and increased surface area improve the dissolution rate of the SCM as well as increase the number of nucleation sites for hydrate precipitation and growth (Skibsted and Snellings, 2019), which translates to higher heat flows in the R^3 protocol. Snellings (Snellings, 2013) described that the rate-controlling step for the dissolution of glasses typically relates to

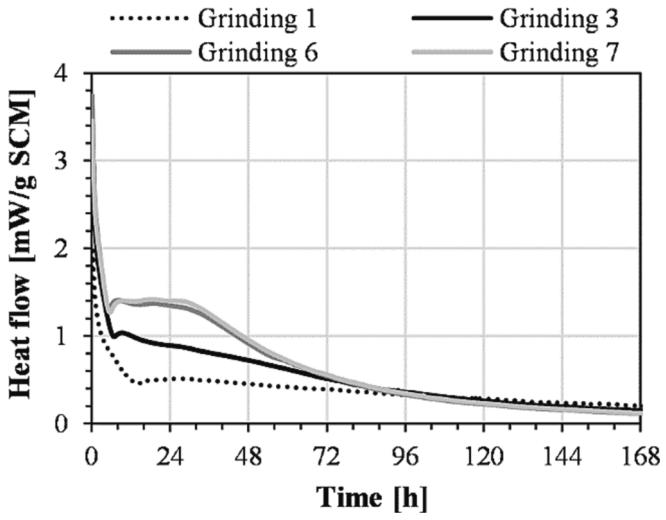

Fig. 9. Heat flow for the first 7 days.

surface-controlled dissolution governed by the formation of surface complexes, diffusion-controlled dissolution limited by diffusion through growing layers of reaction products, and near-surface nucleation and growth rate of hydration products. Increasing the specific surface area should theoretically facilitate faster dissolution for all three mechanisms. Consequently, the minor agglomeration induced by excessive grinding should facilitate the reciprocal relationship. Therefore, the improved reactivity of the SCM from the most extended durations of high-energy grinding should relate to intrinsic differences in the amorphous structure.

The four selected samples, presented in Fig. 9, were subjected to DSC analyses, and the results are reproduced as heat capacity to illustrate the subsequent calculations performed using the data. The first upscan, i.e., studying the behavior of the water-granulated slag subjected to high-energy grinding, generates a C_p curve that is including the endothermic glass transition and exothermic crystallization, as seen in Fig. 10 **a)**. Since the grinding study was performed on subsamples of the same granulated slag, the differences between the samples are mainly attributed to the high-energy grinding. Consequently, by performing a downscan after the first upscan, a similar slowly cooled slag sample that is rid of the effect of grinding and quenching is generated for all four samples. Finally, the subsequent second upscan allows each sample to be compared to a similar baseline heat capacity. By using the heat capacity data from both upscans, integration according to **Eq. (1)** provides a calculation basis for the excessive enthalpy stored in the slag due to the water granulation and grinding. The result for such an integration of the C_p values in Fig. 10 **a)** is illustrated by the solid black line in Fig. 10 **b)**.

$$H = \int_{T_1}^{T_2} (C_{p,2} - C_{p,1}) dT \quad (1)$$

where H is the excessive enthalpy [J/g], T_2 is the high-temperature join of the two C_p curves [K], T_1 is the low-temperature join of the two C_p curves [K], $C_{p,2}$ is the C_p of the second upscan [J/gK], and $C_{p,1}$ is the C_p of the first upscan [J/gK].

Fig. 10 **b)** indicates that the heat of crystallization, integrated between the two C_p curves, generally decreases with increased time of grinding. Furthermore, the endothermic heat related to the glass transition decreased as well. Both observations suggest that the grinding takes the material closer to the equilibrated state in ambient conditions. However, the overall excessive enthalpy increases with prolonged grinding, especially seen when increasing the grinding from 24 to 48 min, which suggests that, on the whole, the material moved further from equilibrium. These observations are consistent with calculations based on DSC measurements of GGBS subjected to high-energy grinding

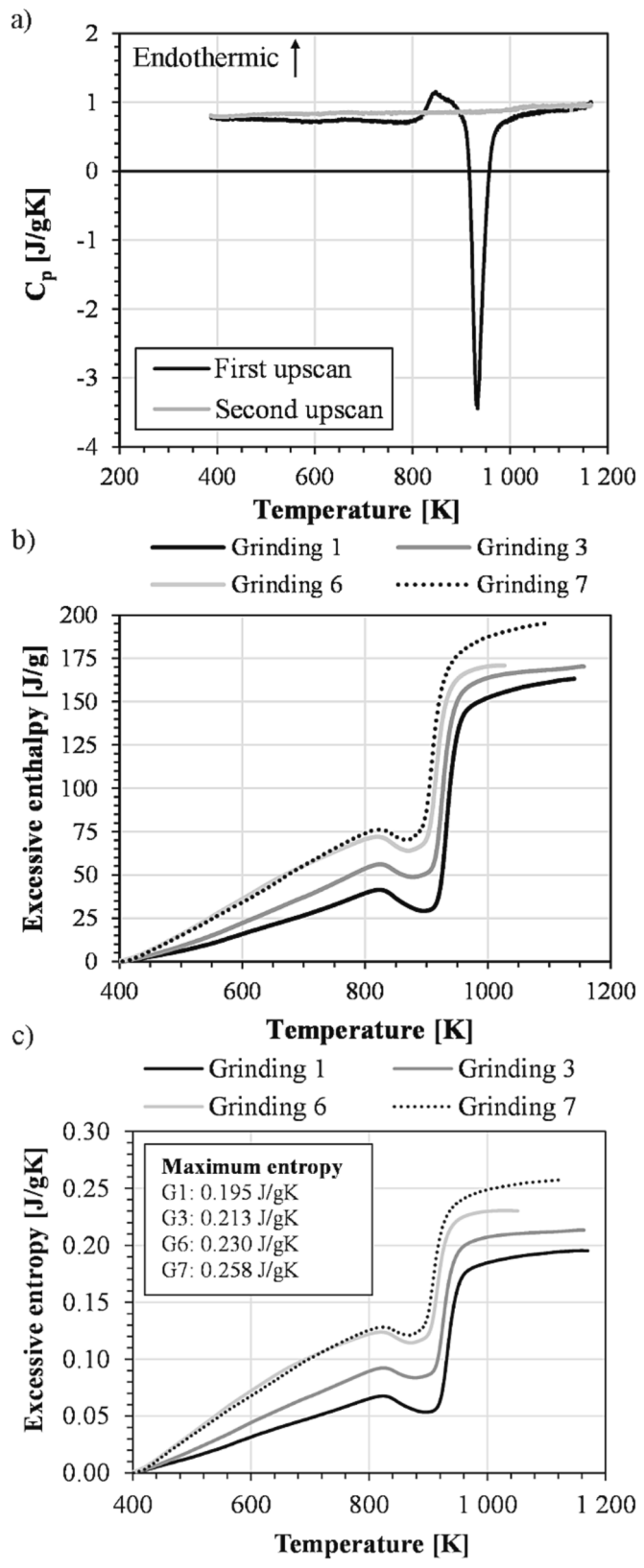

Fig 10. **A)** C_p data for two consecutive upscans for the sample labeled Grinding 1. Calculated **b)** excessive enthalpy and **c)** excessive entropy for the four analyzed samples.

experiments (Romero Sarcos et al., 2021). In their study, Romero Sarcos et al. (Romero Sarcos et al., 2021) motivated the higher potential energy induced by the milling by the formation of highly energetically excited defects being formed on the surface. Furthermore, Shchipalov et al. (Shchipalov et al., 1998) have described that high-intensity glass milling that does not induce particle breakage may influence the bond angle of silicon-oxygen-silicon bonds, translating to higher internal energy of the glass.

Considering the reported explanations for different excessive enthalpies, a more reasonable quantity to evaluate is the excessive entropy, calculated according to **Eq. (2)**. The entropy calculations, Fig. 10**c)**, show consistent differences in accordance with the structural changes proposed by Romero Sarcos (Romero Sarcos et al., 2021) and Shchipalov et al. (Shchipalov et al., 1998). Consequently, the reactivity of the slag may increase by being further from equilibrium and having a larger driving force and potential to overcome kinetic barriers.

$$S = \int_{T_1}^{T_2} \frac{(C_{p,2} - C_{p,1})}{T} dT \tag{2}$$

where S is the excessive entropy [J/gK], T_2 is the high-temperature join of the two C_p curves [K], T_1 is the low-temperature join of the two C_p curves [K], $C_{p,2}$ is the C_p of the second upscan [J/gK], and $C_{p,1}$ is the C_p of the first upscan [J/gK].

3.5. *Effect of granulation temperature*

The idea of changing the granulation temperature was, as briefly covered in **Section 3.3**, based on two previously observed phenomena: i) the changes in the silicate network observed for samples quenched from higher temperatures (Stebbins, 1988), and ii) the relation between thermal history and reactivity (Skibsted and Snellings, 2019). The former aspect concerns observations that increasing the temperature of an oxidic melt with a silicate network has the same structural effect as adding basic oxides (Stebbins, 1988). Furthermore, the polymerization of the silicate network influences the dissolution kinetics of SCMs (Schöler et al., 2017; Snellings, 2013). The second aspect, i.e., the thermal history, relates to the fact that the excessive enthalpy and fictive temperature may be higher in a material granulated from a higher temperature. Fig. 11 illustrates the calculated enthalpy as a function of the temperature of a fully liquid slag with the composition presented in Table 3. These calculations, performed using the GTOX database of FactSage 8.2 (Bale et al., 2016; GTT-Technologies, GTOx Version 17 Documentation, Herzogenrath, 2022; Yazhenskikh et al., 2019), show that the slag has 246 J/g higher enthalpy at the highest temperature

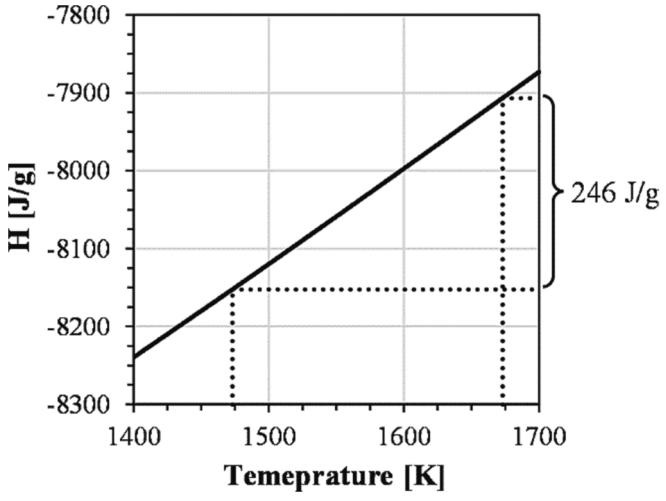

Fig. 11. Calculated enthalpy of the slag.

compared to the lowest temperature of the present study. Therefore, granulating the material from a higher temperature has, theoretically, a possibility to create a material that is thermodynamically more different from its slow-cooled counterpart, i.e., a material that is further from equilibrium in ambient conditions.

Although the previous paragraph indicated that granulation temperature might translate to increased reactivity via two possible mechanisms, the results highlight that this parameter is less critical, Fig. 12. A fair comparison of the three samples requires similar specific surface areas and degrees of crystallinities. The specific surface area was determined to be 0.670, 0.702, and 0.705 m^2/g for the samples 1473 K, 1573 K, and 1673 K, respectively, i.e., consistent between samples. Furthermore, Fig. 13 shows that all three samples were entirely amorphous, analogously to the industrially granulated slag. Snellings and Scrivener (Snellings and Scrivener, 2016) reported that the standard error of the R^3 method was within 2–3 %. Therefore, the tested temperature interval, in combination with the chosen grinding procedure and achieved cooling rate, rendered insignificant differences in the cumulative heat. These results are in line with those for GGBS presented by Ehrenberg (Ehrenberg, 2013), showing that different granulation temperatures have a low impact on the reactivity, provided that crystallization is avoided.

In contrast to the calculations presented in Fig. 11, the DSC analyses showed inconsistent results. Compared to the sample granulated from 1473 K, increasing the temperature by 100 and 200 K generated a change in the excessive enthalpy of −43 J/g and + 33 J/g, respectively. The inconsistent values propose that the contribution of superheating to the excessive enthalpy is ambiguous in the present study. In **Section 3.4**, the purpose of running the DSC was to identify changes posed by the grinding. When studying superheating, the grinding prior to the DSC analyses may have hampered the ability to isolate the phenomenon that was tried to be identified. Romero Sarcos et al. (Romero Sarcos et al., 2021) found that even short grinding periods influenced the C_p curves of GGBS as compared to studying the original granules. Nonetheless, as the milled material is the actual material to be used as an SCM, the methodology used in the present study relates directly to the application. In fact, the variations observed in the DSC measurements follow the slight differences presented in the text box in Fig. 12. Nevertheless, possible inherent changes in the slag induced by superheating have an insignificant effect on the reactivity as opposed to non-breakage effects

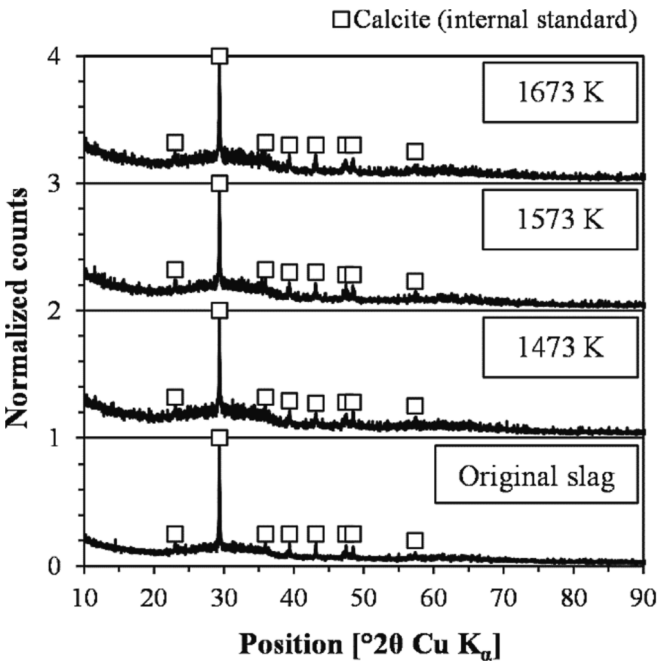

Fig. 13. Diffractograms after granulation in laboratory scale experiments.

introduced by high-energy grinding. A possible reason may be that the two mechanisms outlined in the first paragraph under Section 3.5 did not generate a substantial difference in the granulated slag in the 200 K temperature interval.

Finally, the results presented in Fig. 12 indicate that laboratory scale granulation after remelting in iron crucibles is a suitable method in terms of creating a material that behaves the same way as an industrial slag.

4. Conclusions

In the present study, an iron silicate slag from a copper smelter was studied for its inherent reactivity as an SCM. More specifically, the

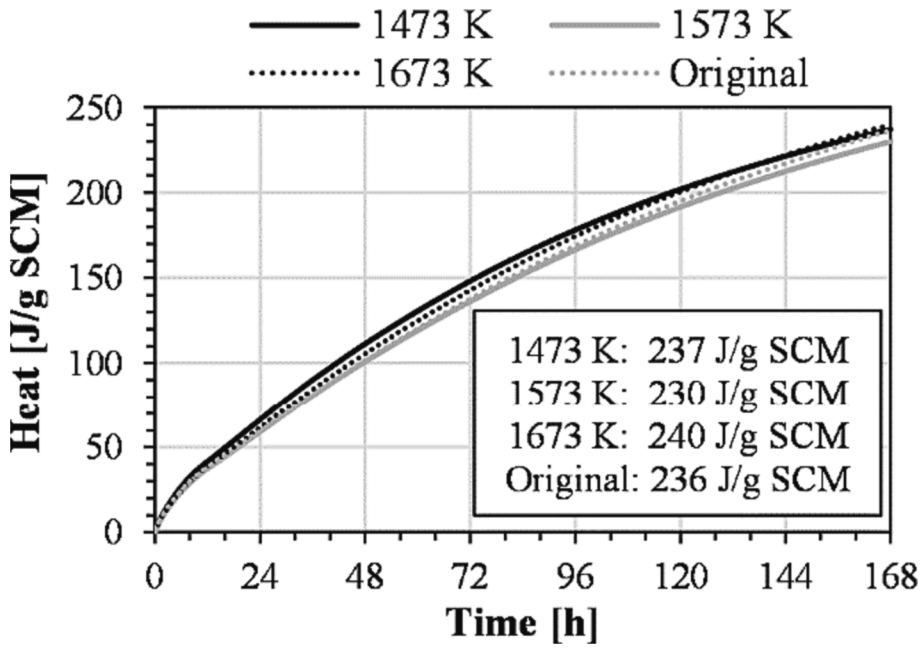

Fig. 12. Cumulative heat vs. time determined by the R^3 protocol. The final 7 day heat is presented in the text box.

influence of prolonged grinding and granulation temperature was investigated, concluding that:

- The particle breakage induced by grinding increases the reactivity of the slag by increasing the specific surface area and the number of sites for nucleation and growth of hydrate products.
- In addition, the grinding generates changes in the slag structure, quantifiable by measuring the excessive enthalpy and entropy, which correlates to a higher reactivity.
- Although a theoretical foundation relating superheating prior to quenching to the resulting reactivity of SCMs is present, the effect is negligible for iron silicate slags at the temperature interval and cooling rate of the present study.

Furthermore, the literature review highlighted the need for controlled studies on the effect of chemical composition on the inherent reactivity of iron silicate copper slags. The granulation experiments using iron crucibles indicated that iron silicate slags granulated in laboratory scale behave similarly to industrially granulated slags, which suggests that laboratory scale experiments can offer a basis for studies on variation in chemical composition.

Declaration of competing interest

The authors declare that they have no known competing financial interests or personal relationships that could have appeared to influence the work reported in this paper.

Data availability

Data will be made available on request.

Acknowledgment

The work was funded by Boliden AB and conducted within the Centre of Advanced Mining and Metallurgy (CAMM) at Luleå University of Technology. The assistance of Britt-Louise Holmqvist is greatly acknowledged.

Role of the funding source

The financial support by Boliden AB was limited to funding, i.e., the participating researchers determined the design of the study, the collection, analysis, and interpretation of data, as well as the writing of the manuscript.

References

Al-Jabri, K.S., Taha, R.A., Al-Hashmi, A., Al-Harthy, A.S., 2006. Effect of copper slag and cement by-pass dust addition on mechanical properties of concrete. Construction and Building Materials 20, 322–331. https://doi.org/10.1016/j.conbuildmat.2005.01.020.

Astoveza, J., Trauchessec, R., Migot-Choux, S., Soth, R., Pontikes, Y., 2022. Iron-rich slag addition in ternary binders of Portland cement, aluminate cement and calcium sulfate. Cement and Concrete Research 153, 106689. https://doi.org/10.1016/j.cemconres.2021.106689.

F. Avet, R. Snellings, A.A. Diaz, M. ben Haha, K. Scrivener, Development of a new rapid, relevant and reliable (R3) test method to evaluate the pozzolanic reactivity of calcined kaolinitic clays, Cem Concr Res. 85 (2016) 1–11. https://doi.org/10.1016/j.cemconres.2016.02.015.

Bale, C.W., Bélisle, E., Chartrand, P., Decterov, S.A., Eriksson, G., Gheribi, A.E., Hack, K., Jung, I.H., Kang, Y.B., Melançon, J., Pelton, A.D., Petersen, S., Robelin, C., Sangster, J., Spencer, P., van Ende, M.A., 2016. Reprint of: FactSage thermochemical software and databases, 2010–2016. Calphad 55, 1–19. https://doi.org/10.1016/j.calphad.2016.07.004.

Benhelal, E., Shamsaei, E., Rashid, M.I., 2021. Challenges against CO_2 abatement strategies in cement industry: A review. Journal of Environmental Sciences 104, 84–101. https://doi.org/10.1016/j.jes.2020.11.020.

Bignozzi, M.C., Saccani, A., Barbieri, L., Lancellotti, I., 2015. Glass waste as supplementary cementing materials: The effects of glass chemical composition. Cement and Concrete Composites 55, 45–52. https://doi.org/10.1016/j.cemconcomp.2014.07.020.

de Rojas, M.I.S., Rivera, J., Frías, M., Marín, F., 2008. Use of recycled copper slag for blended cements. Journal of Chemical Technology and Biotechnology 83, 209–217. https://doi.org/10.1002/jctb.1830.

Edwin, R.S., de Schepper, M., Gruyaert, E., de Belie, N., 2016. Effect of secondary copper slag as cementitious material in ultra-high performance mortar. Construction and Building Materials 119, 31–44. https://doi.org/10.1016/j.conbuildmat.2016.05.007.

Ehrenberg, A., 2013. Influence of the granulation conditions and performance potential of granulated blastfurnace slag-Part 2: Chemistry and physical properties. ZKG International. 3, 60–67.

Feng, Y., Kero, J., Yang, Q., Chen, Q., Engström, F., Samuelsson, C., Qi, C., 2019. Mechanical Activation of Granulated Copper Slag and Its Influence on Hydration Heat and Compressive Strength of Blended Cement. Materials. 12, 772. https://doi.org/10.3390/ma12050772.

Feng, Y., Yang, Q., Chen, Q., Kero, J., Andersson, A., Ahmed, H., Engström, F., Samuelsson, C., 2019. Characterization and evaluation of the pozzolanic activity of granulated copper slag modified with CaO. Journal of Cleaner Production 232, 1112–1120. https://doi.org/10.1016/j.jclepro.2019.06.062.

Gabasiane, T.S., Danha, G., Mamvura, T.A., Mashifana, T., Dzinomwa, G., 2021. Environmental and Socioeconomic Impact of Copper Slag—A Review. Crystals 11, 1–16. https://doi.org/10.3390/cryst11121504.

Gholizadeh Vayghan, A., Horckmans, L., Snellings, R., Peys, A., Teck, P., Maier, J., Friedrich, B., Klejnowska, K., 2021. Use of treated non-ferrous metallurgical slags as supplementary cementitious materials in cementitious mixtures. Applied Sciences 11, 4028. https://doi.org/10.3390/app11094028.

Glosser, D., Suraneni, P., Isgor, O.B., Weiss, W.J., 2021. Using glass content to determine the reactivity of fly ash for thermodynamic calculations. Cement and Concrete Composites 115, 103849. https://doi.org/10.1016/j.cemconcomp.2020.103849.

Grazulis, S., Chateigner, D., Downs, R.T., Yokochi, A.F.T., Quirós, M., Lutterotti, L., Manakova, E., Butkus, J., Moeck, P., le Bail, A., 2009. Crystallography Open Database - an open-access collection of crystal structures. Journal of Applied Crystallography 42, 726–729. https://doi.org/10.1107/S0021889809016690.

GTT-Technologies, GTOx Version 17 Documentation, Herzogenrath, 2022.

Hallet, V., de Belie, N., Pontikes, Y., 2020. The impact of slag fineness on the reactivity of blended cements with high-volume non-ferrous metallurgy slag. Construction and Building Materials 257, 119400. https://doi.org/10.1016/j.conbuildmat.2020.119400.

He, R., Zhang, S., Zhang, X., Zhang, Z., Zhao, Y., Ding, H., 2021. Copper slag: The leaching behavior of heavy metals and its applicability as a supplementary cementitious material. Journal of Environmental Chemical Engineering 9, 105132. https://doi.org/10.1016/j.jece.2021.105132.

Hertwich, E.G., 2021. Increased carbon footprint of materials production driven by rise in investments. Nature Geoscience 14, 151–155. https://doi.org/10.1038/s41561-021-00690-8.

International Copper Study Group, The World Copper Factbook, 2022. Lisbon. Portugal 2022, 25.

Isaksson, J., Vikström, T., Lennartsson, A., Andersson, A., Samuelsson, C., 2021. Settling of Copper Phases in Lime Modified Iron Silicate Slag. Metals. 11, 1098. https://doi.org/10.3390/met11071098.

Kero Andertun, J., Samuelsson, C., Peltola, P., Engström, F., 2022. Characterisation and leaching behaviour of granulated iron silicate slag constituents. Canadian Metallurgical Quarterly 61, 14–23. https://doi.org/10.1080/00084433.2021.2016345.

Kero Andertun, J., Peltola, P., Engström, F., Samuelsson, C., 2022. The Effect of Zn Content and Granulation Temperature on Zn Leaching in an Fe-Saturated (FeXZn (1−X))2SiO4 System. Minerals. 12, 767. https://doi.org/10.3390/min12060767.

Kucharczyk, S., Sitarz, M., Zajac, M., Deja, J., 2018. The effect of CaO/SiO_2 molar ratio of CaO-Al_2O_3-SiO_2 glasses on their structure and reactivity in alkali activated system. Spectrochimica Acta. Part A, Molecular and Biomolecular Spectroscopy 194, 163–171. https://doi.org/10.1016/j.saa.2018.01.018.

Li, X., Snellings, R., Antoni, M., Alderete, N.M., M. ben Haha, S. Bishnoi, Ö. Cizer, M. Cyr, K. de Weerdt, Y. Dhandapani, J. Duchesne, J. Haufe, D. Hooton, M. Juenger, S. Kamali-Bernard, S. Kramar, M. Marroccoli, A.M. Joseph, A. Parashar, C. Patapy, J.L. Provis, S. Sabio, M. Santhanam, L. Steger, T. Sui, A. Telesca, A. Vollpracht, F. Vargas, B. Walkley, F. Winnefeld, G. Ye, M. Zajac, S. Zhang, K.L. Scrivener,, 2018. Reactivity tests for supplementary cementitious materials. Materials and Structures 51, 1–14. https://doi.org/10.1617/s11527-018-1269-x. RILEM TC 267-TRM phase 1,.

Lothenbach, B., Scrivener, K., Hooton, R.D., 2011. Supplementary cementitious materials. Cement and Concrete Research 41, 1244–1256. https://doi.org/10.1016/j.cemconres.2010.12.001.

Mirzahosseini, M., Riding, K.A., 2015. Influence of different particle sizes on reactivity of finely ground glass as supplementary cementitious material (SCM). Cement and Concrete Composites 56, 95–105. https://doi.org/10.1016/j.cemconcomp.2014.10.004.

Moon, G.D., Oh, S., Choi, Y.C., 2016. Effects of the physicochemical properties of fly ash on the compressive strength of high-volume fly ash mortar. Construction and Building Materials 124, 1072–1080. https://doi.org/10.1016/j.conbuildmat.2016.08.148.

Moura, W.A., Gonçalves, J.P., Lima, M.B.L., 2007. Copper slag waste as a supplementary cementing material to concrete. Journal of Materials Science 42, 2226–2230. https://doi.org/10.1007/s10853-006-0997-4.

Murari, K., Siddique, R., Jain, K.K., 2015. Use of waste copper slag, a sustainable material. Journal of Material Cycles and Waste Management 17, 13–26. https://doi.org/10.1007/s10163-014-0254-x.

Mysen, B., Richet, P., 2018. Silicate glasses and melts, 2nd ed. Elsevier.
J.G.J. Olivier, G. Janssens-Maenhout, J.A.H.W. Peters, Trends in global CO_2 emissions; 2012 Report, PBL Netherlands Environmental Assessment Agency, 2012.
Peys, A., Isteri, V., Yliniemi, J., Yorkshire, A.S., Lemougna, P.N., Utton, C., Provis, J.L., Snellings, R., Hanein, T., 2022. Sustainable iron-rich cements: Raw material sources and binder types. Cement and Concrete Research 157, 106834. https://doi.org/10.1016/j.cemconres.2022.106834.
Ramanathan, S., Perumal, P., Illikainen, M., Suraneni, P., 2021. Mechanically activated mine tailings for use as supplementary cementitious materials. RILEM Technical Letters. 6, 61–69. https://doi.org/10.21809/rilemtechlett.2021.143.
Ramanathan, S., Tuen, M., Suraneni, P., 2022. Influence of supplementary cementitious material and filler fineness on their reactivity in model systems and cementitious pastes. Materials and Structures 55, 1–25. https://doi.org/10.1617/s11527-022-01980-2.
Romero Sarcos, N., Hart, D., Bornhöft, H., Ehrenberg, A., Deubener, J., 2021. Rejuvenation of granulated blast furnace slag (GBS) glass by ball milling. Journal of Non-Crystalline Solids 556, 120557. https://doi.org/10.1016/j.jnoncrysol.2020.120557.
Schöler, A., Winnefeld, F., M. ben Haha, B. Lothenbach,, 2017. The effect of glass composition on the reactivity of synthetic glasses. Journal of the American Ceramic Society 100, 2553–2567. https://doi.org/10.1111/jace.14759.
Shchipalov, Y.K., Osokin, A.K., Gusarov, A.M., Tumanova, S.E., 1998. The effect of cullet grinding in impact-repulsion mills on the properties of glass powders. Glass and Ceramics 55, 344–348.
Sheng, G., Wang, B., Wang, S., Wang, Z., 2016. Pozzolanic Reaction of FeO-SiO_2 Slag with Portlandite. J Solid Waste Technol Manage. 42, 51–57. https://doi.org/10.5276/JSWTM.2016.51.
Shi, C., Wu, Y., Riefler, C., Wang, H., 2005. Characteristics and pozzolanic reactivity of glass powders. Cement and Concrete Research 35, 987–993. https://doi.org/10.1016/j.cemconres.2004.05.015.
Shi, C., Meyer, C., Behnood, A., 2008. Utilization of copper slag in cement and concrete. Resources, Conservation and Recycling 52, 1115–1120. https://doi.org/10.1016/j.resconrec.2008.06.008.
Singh, J., Singh, J., Kaur, M., 2016. Copper Slag Blended Cement: An Environmental Sustainable Approach for Cement Industry in India. Current World Environment: An International Research Journal of Environmental Sciences 11, 186–193. https://doi.org/10.12944/cwe.11.1.23.
P.P. Sivakumar, E. Gruyaert, N. de Belie, S. Matthys, REACTIVITY OF MODIFIED IRON SILICATE SLAG AS SUSTAINABLE ALTERNATIVE BINDER, in: Fifth International Conference on Sustainable Construction Materials and Technologies, International Committee of the SCMT conferences, 2019: pp. 39–49.
Sivakumar, P.P., Matthys, S., de Belie, N., Gruyaert, E., 2021. Reactivity Assessment of Modified Ferro Silicate Slag by R3 Method. Applied Sciences 11, 1–14. https://doi.org/10.3390/app11010366.
Skibsted, J., Snellings, R., 2019. Reactivity of supplementary cementitious materials (SCMs) in cement blends. Cement and Concrete Research 124, 105799. https://doi.org/10.1016/j.cemconres.2019.105799.
Snellings, R., 2013. Solution-Controlled Dissolution of Supplementary Cementitious Material Glasses at pH 13: The Effect of Solution Composition on Glass Dissolution Rates. Journal of the American Ceramic Society 96, 2467–2475. https://doi.org/10.1111/jace.12480.
Snellings, R., Scrivener, K.L., 2016. Rapid screening tests for supplementary cementitious materials: past and future. Materials and Structures 49, 3265–3279. https://doi.org/10.1617/s11527-015-0718-z.
Stebbins, J.F., 1988. Effects of temperature and composition on silicate glass structure and dynamics: Si-29 NMR results. Journal of Non-Crystalline Solids 106, 359–369.
Tian, M., Wan, X., Chen, M., Taskinen, P., Tiljander, M., Jokilaakso, A., 2022. Phase equilibria of FeOx-SiO2-Al2O3 slag system at 1200 °C and pO2 of 10–8.6 atm. Calphad 79, 102502. https://doi.org/10.1016/j.calphad.2022.102502.
Tixier, R., Devaguptapu, R., Mobasher, B., 1997. THE EFFECT OF COPPER SLAG ON THE HYDRATION AND MECHANICAL PROPERTIES OF CEMENTITIOUS MIXTURES. Cement and Concrete Research 27, 1569–1580.
Wang, D., Wang, Q., Huang, Z., 2020. Reuse of copper slag as a supplementary cementitious material: Reactivity and safety. Resources, Conservation and Recycling 162, 105037. https://doi.org/10.1016/j.resconrec.2020.105037.
Watari, T., Northey, S., Giurco, D., Hata, S., Yokoi, R., Nansai, K., Nakajima, K., 2022. Global copper cycles and greenhouse gas emissions in a 1.5 °C world. Resources, Conservation and Recycling 179, 106118. https://doi.org/10.1016/j.resconrec.2021.106118.
Yao, G., Cui, T., Zhang, J., Wang, J., Lyu, X., 2020. Effects of mechanical grinding on pozzolanic activity and hydration properties of quartz. Advanced Powder Technology 31, 4500–4509. https://doi.org/10.1016/j.apt.2020.09.028.
Yazhenskikh, E., Jantzen, T., Hack, K., Müller, M., 2019. A new multipurpose thermodynamic database for oxide systems. Rasplawy. 2, 116–124.
Zhang, Y., Wan, Z., de Lima Junior, L.M., Çopuroğlu, O., 2022. Early age hydration model of slag cement: Interaction among C_3S, gypsum and slag with different Al_2O_3 contents. Cement and Concrete Research. 161, 106954 https://doi.org/10.1016/j.cemconres.2022.106954.
Zhang, T.S., Yu, Q.J., Wei, J.X., Zhang, P.P., 2011. Effect of size fraction on composition and pozzolanic activity of high calcium fly ash. Advances in Cement Research 23, 299–307. https://doi.org/10.1680/adcr.2011.23.6.299.